The Equatorial Pacific Cold Tongue Bias in a Coupled Climate Model

VASUBANDHU MISRA* AND L. MARX

Institute of Global Environment and Society, Center for Ocean–Land–Atmosphere Studies, Calverton, Maryland

M. BRUNKE AND X. ZENG

Department of Atmospheric Science, The University of Arizona, Tucson, Arizona

(Manuscript received 21 August 2007, in final form 14 February 2008)

ABSTRACT

A set of multidecadal coupled ocean–atmosphere model integrations are conducted with different time steps for coupling between the atmosphere and the ocean. It is shown that the mean state of the equatorial Pacific does not change in a statistically significant manner when the coupling interval between the atmospheric general circulation model (AGCM) and the ocean general circulation model (OGCM) is changed from 1 day to 2 or even 3 days. It is argued that because the coarse resolution of the AGCM precludes resolving realistic "weather" events, changing the coupling interval from 1 day to 2 or 3 days has very little impact on the mean coupled climate.

On the other hand, reducing the coupling interval to 3 h had a much stronger impact on the mean state of the equatorial Pacific and the concomitant general circulation. A novel experiment that incorporates a (pseudo) interaction of the atmosphere with SST at every time step of the AGCM was also conducted. In this unique coupled model experiment, the AGCM at every time step mutually interacts with the skin SST. This skin SST is anchored to the bulk SST, which is updated from the OGCM once a day. Both of these experiments reduced the cold tongue bias moderately over the equatorial Pacific Ocean with a corresponding reduction in the easterly wind stress bias relative to the control integration. It is stressed from the results of these model experiments that the impact of high-frequency air–sea coupling is significant on the cold tongue bias.

The interannual variation of the equatorial Pacific was less sensitive to the coupling time step between the AGCM and the OGCM. Increasing (reducing) the coupling interval of the air–sea interaction had the effect of weakening (marginally strengthening) the interannual variations of the equatorial Pacific Ocean.

It is argued that the low-frequency response of the upper ocean, including the cold tongue bias, is modulated by the atmospheric stochastic forcing on the coupled ocean–atmosphere system. This effect of the atmospheric stochastic forcing is affected by the frequency of the air–sea coupling and is found to be stronger than the rectification effect of the diurnal variations of the air–sea interaction on the low frequency. This may be a result of a limitation in the coupled model used in this study in which the OGCM has an inadequate vertical resolution in the mixed layer to sustain diurnal variations in the upper ocean.

1. Introduction

The equatorial Pacific cold tongue bias [also commonly referred to as the double or split intertropical convergence zone (ITCZ)] in coupled climate models has prevailed for nearly two decades (Mechoso et al. 1995; Latif et al. 2001; Randall et al. 2007). It also deteriorates El Niño–Southern Oscillation (ENSO) variability (Misra et al. 2008; Latif et al. 2001). This double ITCZ is associated with spurious precipitation south of the equator with concomitant warm SST bias.

There have been several efforts to ameliorate this problem in the climate models. By imposing an annually varying stratus cloud amount off the coast of Peru, Yu and Mechoso (1999) reduced this cold tongue bias considerably. Zhang and Mu (2005) and Zhang and Wang (2006) made some significant improvements in

* Current affiliation: Department of Meteorology, and Center for Ocean–Atmosphere Prediction Studies, The Florida State University, Tallahassee, Florida.

Corresponding author address: Vasubandhu Misra, Department of Meteorology, The Florida State University, 404 Love Building, Tallahassee, FL 32312.
E-mail: vmisra@fsu.edu

DOI: 10.1175/2008JCLI2205.1

the double-ITCZ problem through a change in the closure of the Zhang and McFarlane (1995) convection scheme. They made the change in the closure of the scheme to make it depend on the large-scale forcing of the free troposphere rather than the convectively available potential energy. Similarly, aquaplanet experiments have provided useful insight into the cold tongue issue (Sumi 1992; Kirtman and Schneider 2000; Chao and Chen 2004). These theoretical studies showed the importance of the Coriolis force and the role of the convective parameterization scheme in locating the ITCZ in the deep tropics. In this study we will be addressing this issue of the cold tongue bias in the context of its sensitivity to the frequency of the coupling between the atmospheric general circulation model (AGCM) and the ocean general circulation model (OGCM).

This study is focused on questioning the validity of a popular choice of coupling the AGCM and the OGCM of a coupled climate model once a day. In a recent evaluation of the Intergovernmental Panel for Climate Change (IPCC) models it was found that a majority of them had a coupling interval of 1 day (Randall et al. 2007). This choice of a 1-day coupling interval becomes even more intriguing after the fact that most of these climate models have been found to be inadequate to represent subseasonal variations, including the Madden–Julian oscillation (MJO) and synoptic variability (Sperber et al. 2005; Zhang 2005; Lin et al. 2006; Randall et al. 2007). Furthermore, the coarse resolution of the AGCM in the current models has been dismissed for operational weather forecasting. The horizontal resolution of the numerical weather prediction models over the last decade has increased several fold, with the National Centers for Environmental Prediction (NCEP) and the European Centre for Medium-Range Weather Forecasts (ECMWF) adopting spectral resolutions of T382 and T799 for their global models, which translates to about 0.3° and 0.15° grid resolution, respectively. Their regional models are run at an even higher resolution. Therefore, it further begs the following question: is the coupling interval of 1 day between the AGCM and the OGCM really an optimal choice for the current coarsely resolved climate models?

There might be four reasons for the choice of a 1-day coupling interval, as delineated below:

1) Most current models either use a Julian or a Gregorian calendar that has 12 months (with irregular number of days from one month to the next), which makes the once-a-day coupling interval most convenient. For example, in choosing longer intervals of coupling (say 2 or 3 days) it becomes cumbersome to run the coupled model, especially when it is made to restart after every month of integration. Thus, all of the flux terms would have to be stored in the restart files in order to compute the correct average of the forcing for the component models.
2) The best compromise of the available resources is between the desire to have the highest possible coupling frequency that will best mimic nature (which displays a continuum in air-sea interaction) and the desire to develop the climate model with more sophisticated physics, more climate components, the addition of more ensemble members, and the push for modest increases in model resolution.
3) There is a practical limitation to the numerics and reconciliation with approximations in the climate model, such as invoking the radiation calculation at relatively large time intervals and the use of parameterized schemes that depend on time-averaged quantities (Randall et al. 2007; Danabasoglu et al. 2006; Brunke et al. 2003).
4) Despite the coarse resolution of the climate models, some studies point to the importance of the noise statistics arising from the internal dynamics of the component models (AGCM and OGCM) in modulating the coupled variability from seasons to decades (Kirtman and Shukla 2002; Kirtman et al. 2005; Wu et al. 2004; Sura and Penland 2002).

This study uses the Center for Ocean–Land–Atmosphere Studies (COLA) coupled model, version 3.2 (Misra et al. 2007). This model's mean climate and interannual variations are reasonable. It has been widely used for climate studies (Misra and Marx 2007; Misra et al. 2007; Cash et al. 2007; Delsole et al. 2008).

In some related studies of Bernie et al. (2005, 2007) and Danabasoglu et al. (2006) it is shown that the diurnal variability of the upper ocean has important implications on the MJO and the ENSO variability in addition to its impact on the cold bias of the equatorial Pacific Ocean. Most current coupled climate models preclude the diurnal variations in the upper ocean for at least the following two reasons:

1) The coupling interval between the OGCM and the AGCM is once a day.
2) The vertical resolution in the upper ocean is too coarse (typically around 10 m thick).

The second point in the above is also a limiting factor in the experimental setup of our study with 10-m-thick layers near the ocean surface in the OGCM. However, their idealized model experiments with a double-gyre ocean model, Sura and Penland (2002) show in that its response is sensitive to the details of the atmospheric stochastic forcing. It is suggested in their study that it is possible to modulate the low-frequency response of the

ocean model by simply changing the frequency of the atmospheric stochastic forcing that is applied to the ocean model.

One of the experiments that we conduct in this study is to couple the AGCM to the skin SST rather than to the bulk SST produced by the OGCM. The bulk SST, which is often used both for validation and to force the AGCM, is typically measured between 3 and 5 m below the sea surface (Webster et al. 1996). For a region of the Tropical Ocean and Global Atmosphere Coupled Ocean–Atmosphere Response Experiment (TOGA COARE), the difference between skin and bulk temperature can be as large as 3 K, although it is usually within 1 K (Fairall et al. 1996a). Furthermore, the amplitude of the diurnal cycle of skin temperature, which is on average 0.65 K, can be as high as 2.8 K over the TOGA Tropical Atmosphere Ocean (TAO) buoy array (Zeng et al. 1999). Fairall et al. (1996b) indicate that to obtain bulk surface estimates within ± 10 W m^{-2}, the bulk SSTs have to be corrected for the warm layer and cool skin effects to obtain the skin temperature. The warm layer effect occurs in the upper few meters of the ocean during the day when temperature stratification caused by solar flux absorption leads to suppression of shear-induced mixing. The cool skin effect is almost always present and occurs in the upper few millimeters of the ocean caused by cooling from net longwave radiative, sensible and heat fluxes.

The paper is organized as follows: We will describe the model used in this study in section 2, followed by the description of the experiments conducted in section 3; the results are presented in section 4 with conclusions in section 5.

2. Model description

The COLA coupled climate model (Misra et al. 2007) comprises the AGCM, version 3.2 at a spectral resolution of T62, with 28 terrain-following sigma ($= p/p_s$) levels that are identical to the NCEP–National Center for Atmospheric Research (NCAR) reanalysis model (Kalnay et al. 1996). The dynamical core follows from the Eulerian core of the Community Climate Model, version 3 (Kiehl et al. 1998), wherein all of the dependent variables are spectrally treated, except for moisture, which is advected by a semi-Lagrangian scheme. The relaxed Arakawa–Schubert scheme (Moorthi and Suarez 1992; modified as in Bacmeister et al. 2000) is used for deep convective parameterization. The longwave and shortwave radiation scheme is identical to that in the Community Climate System Model, version 3.0 (Collins et al. 2006). The cloud optical properties follow from Kiehl et al. (1998). The planetary boundary layer is a nonlocal scheme (Hong and Pan 1996) and the shallow convection uses the formulation in Tiedtke (1984). The land surface scheme uses the Simplified Simple Biosphere Model (SSiB; see Xue et al. 1991, 1996; Dirmeyer and Zeng 1999).

This COLA AGCM is coupled to the Modular Ocean Model, version 3.0 (MOM3; Pacanowski and Griffies 1998). MOM3 covers the global oceans between 74°S and 65°N with realistic bottom topography. However, ocean depths less than 100 m are set to 100 m and the maximum depth is 6000 m. The artificial high-latitude meridional boundaries are impermeable and insulating. It has a uniform zonal resolution of 1.5° while the meridional resolution is 0.5° between 10°S and 10°N, gradually increasing to 1.5° at 30°N and 30°S and fixed at 1.5° in the extratropics. The vertical mixing is the nonlocal K-profile parameterization of Large et al. (1994). The momentum mixing uses the space–time-dependent scheme of Smagorinsky (1963), and tracer mixing follows the Redi (1982) and Gent and McWilliams (1990) quasi-adiabatic stirring.

In the control COLA coupled model simulation the daily averaged atmospheric fluxes computed by the AGCM are passed to the OGCM once a day where it is linearly interpolated to its grid. Likewise, the daily averaged SST from the OGCM is passed to the AGCM at intervals of 1 day. In this way, the use of a flux coupler is avoided.

3. Design of the experiments

In all, five coupled multidecadal integrations are conducted for a period of 50 yr. The initial state of the ocean and the atmosphere are borrowed from the end of a previous coupled integration (Misra et al. 2007). The ocean initial condition is therefore well spun up and is in balance with the climate of the COLA coupled model. The CO_2 concentration is a constant 345 ppm, as in present-day control runs. Four of the five model integrations are as follows:

1) CON: uses the control COLA coupled model described in section 2;
2) E2D: uses the identical AGCM and OGCM as those in CON, but the coupling interval between them is changed from 1 day to 2 days; the atmospheric fluxes, including wind stress and SST from the OGCM, are averaged over a period of 2 days before they are exchanged to the respective component models;
3) E3D: the same as E2D, but the coupling interval between the AGCM and the OGCM is changed to 3 days; and
4) E3H: the same as E2D, but the coupling interval is changed to 3 h.

TABLE 1. Description of symbols and parameter values (in brackets) of the skin SST algorithm in Eqs. (1) and (2).

Symbol	Description
δ	Oceanic molecular sublayer depth
T_s	Surface temperature
T_δ	Temperature at the depth of the skin layer
ρ_w	Density of seawater (1025 kg m^{-3})
c_w	Volumetric heat capacity of water (4190 J kg^{-1} K^{-1})
k_w	Molecular thermal conductivity (1.4e^{-7} m^2 s^{-1})
Q	Sum of sensible, latent, and net longwave fluxes
R_s	Net solar radiative flux at the surface
R_{-d}	Net solar radiative flux at the bulk layer depth
f_s	Fraction of solar radiation absorbed in the sublayer
d	Bulk temperature depth (3 m)
υ	Empirical parameter (0.3)
u_{*w}	Friction velocity in water
$\phi_t\left(\frac{d}{L}\right)$	Stability function dependent on Monin–Obukhov length (L)

To facilitate easier manipulation of the coupling interval, we have resorted to using a 360-day calendar with twelve 30-day months for all of the model integrations discussed in this study. The astronomy in the COLA model is based on Berger (1978), so changes to the astronomy resulting from calendar changes are easily made. It should be noted that the model characteristics of the CON integration, such as its mean and the interannual variations over the global tropics, are similar to a corresponding integration from the same model using a 365-day calendar used in Misra et al. (2007).

The fifth model integration discussed in this study is called ESKIN. Here, the AGCM interacts with skin SST that is derived from the bulk SST of the OGCM. The coupling interval between the AGCM and the OGCM is once a day, as in CON. The bulk SST is therefore updated once a day. However, the heat flux and wind stress evolving at each time step of the AGCM is used to derive the skin temperature as a function of the bulk temperature following Zeng and Beljaars (2005). The formulation of the skin SST follows from a simple one-dimensional heat transfer equation that takes the form of

$$\frac{\partial(T_{-\delta} - T_{-d})}{\partial t} = \frac{(Q + R_s - R_{-d})(\upsilon + 1)}{d\rho_\omega c_\omega \upsilon} - \frac{(\upsilon + 1)ku_{*\omega}(T_{-\delta} - T_{-d})}{d\phi_t\left(\frac{d}{L}\right)} \quad (1)$$

for the warm layer temperature difference. Likewise, for the cool skin layer effect, the equation is given by

$$T_s - T_{-\delta} = \frac{\delta}{\rho_\omega c_\omega k_\omega}(Q + R_s f_s). \quad (2)$$

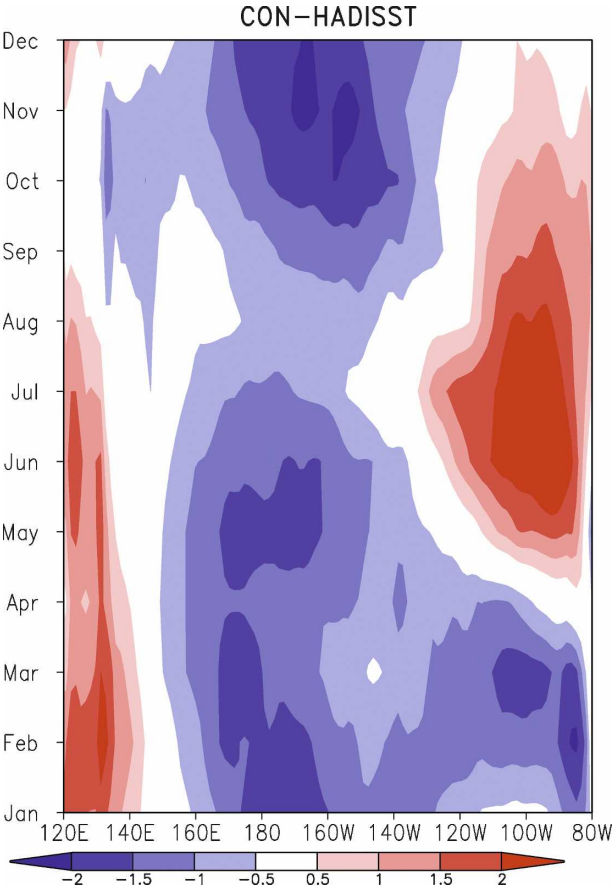

FIG. 1. The climatological monthly mean errors of SST over the equatorial Pacific (averaged between 5°S and 5°N) from CON as compared to HadISST1.1.

The meaning of the symbols and the values of the parameters used in the algorithm are provided in Table 1. More details on this algorithm and the choice of parameter values are given in Zeng and Beljaars (2005).

The first three experiments—CON, E2D, and E3D—are designed to examine whether the once-a-day coupling interval between the AGCM and the OGCM is an optimal choice in the COLA model. The last two experiments—E3H and ESKIN—are designed to resolve the diurnal scales in air–sea coupling in two different ways to examine their impact on the evolution of the coupled climate.

4. Results

To validate the SST from the model simulations we use the Hadley Centre Global Sea Ice and Sea Surface Temperature, version 1.1 (HadISST1.1) data (Rayner et al. 2003) from 1951 to 2000. To validate the subsurface ocean variables we make use of the NCEP Global Ocean Data Assimilation System (GODAS; in-

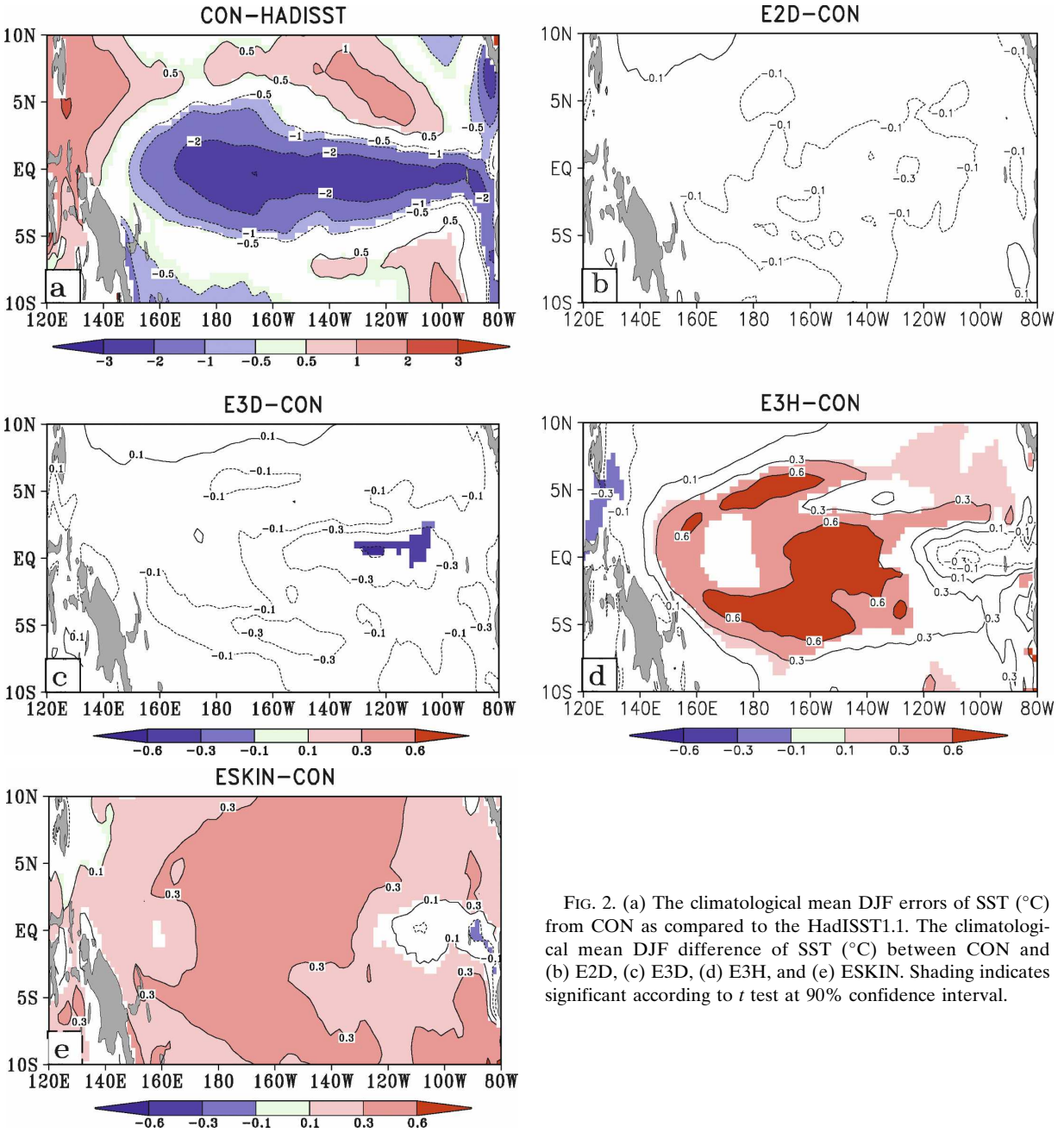

FIG. 2. (a) The climatological mean DJF errors of SST (°C) from CON as compared to the HadISST1.1. The climatological mean DJF difference of SST (°C) between CON and (b) E2D, (c) E3D, (d) E3H, and (e) ESKIN. Shading indicates significant according to t test at 90% confidence interval.

formation available online at http://www.cpc.ncep.noaa.gov/products/GODAS/background.shtml). This is available for a 26-yr period from 1980 to 2006. In GODAS the ocean assimilation is conducted with MOM3, but with a higher horizontal [0.5° in the zonal direction and ⅓° in the meridional direction] and vertical (40 levels) resolution than those used in our model experiments (Misra et al. 2007).

The analysis of the model results are centered over the equatorial Pacific Ocean because it has the most pronounced cold tongue bias in the COLA model. Furthermore, we shall be focusing on the December–February (DJF) season, because it is found to be one of the most severely affected by this cold tongue bias. This is illustrated in Fig. 1, which shows the time–longitude cross section of the climatological monthly mean SST errors over the equatorial Pacific region in the CON experiment. In DJF, the cold bias is nearly zonally symmetric from the central to the eastern equatorial Pacific Ocean. It should be noted that in the following description of the results only bulk SST will be used (even while analyzing the ESKIN experiment).

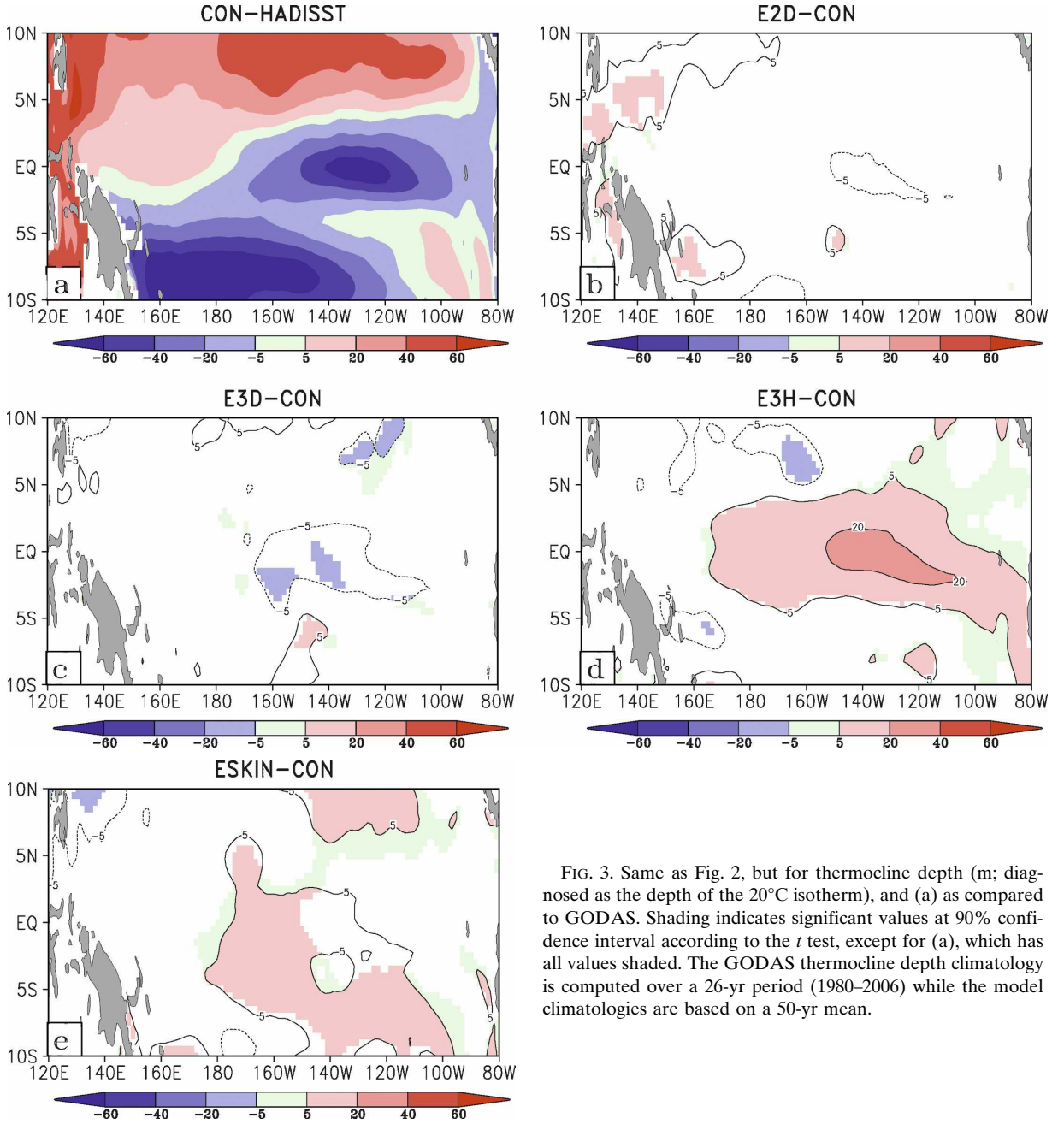

FIG. 3. Same as Fig. 2, but for thermocline depth (m; diagnosed as the depth of the 20°C isotherm), and (a) as compared to GODAS. Shading indicates significant values at 90% confidence interval according to the *t* test, except for (a), which has all values shaded. The GODAS thermocline depth climatology is computed over a 26-yr period (1980–2006) while the model climatologies are based on a 50-yr mean.

a. SST bias

In Fig. 2a the climatological mean DJF SST error of CON is shown. The bias is computed with respect to the HadISST1.1. This figure clearly shows the cold bias is nearly spanning the equatorial Pacific Ocean. The bias is in excess of 2°C over the central and western equatorial Pacific Ocean. This error is comparable to many of the current coupled climate models (Latif et al. 2001; Luo et al. 2005; Saha et al. 2006; Rao and Sperber 2006).

Because the coupling interval between the OGCM and the AGCM is changed to 2 days, as in E2D, the cold tongue bias increases slightly, but its difference from the CON is statistically insignificant at the 90% level (Fig. 2b). This error is further accentuated in E3D when the coupling interval is 3 days (Fig. 2c), but the differences between E3D and CON are statistically insignificant for the most part. In E3H (Fig. 2d), when the coupling interval is reduced to 3 h, there is a widespread reduction of the cold bias over the equatorial Pacific Ocean. Likewise, in the ESKIN experiment

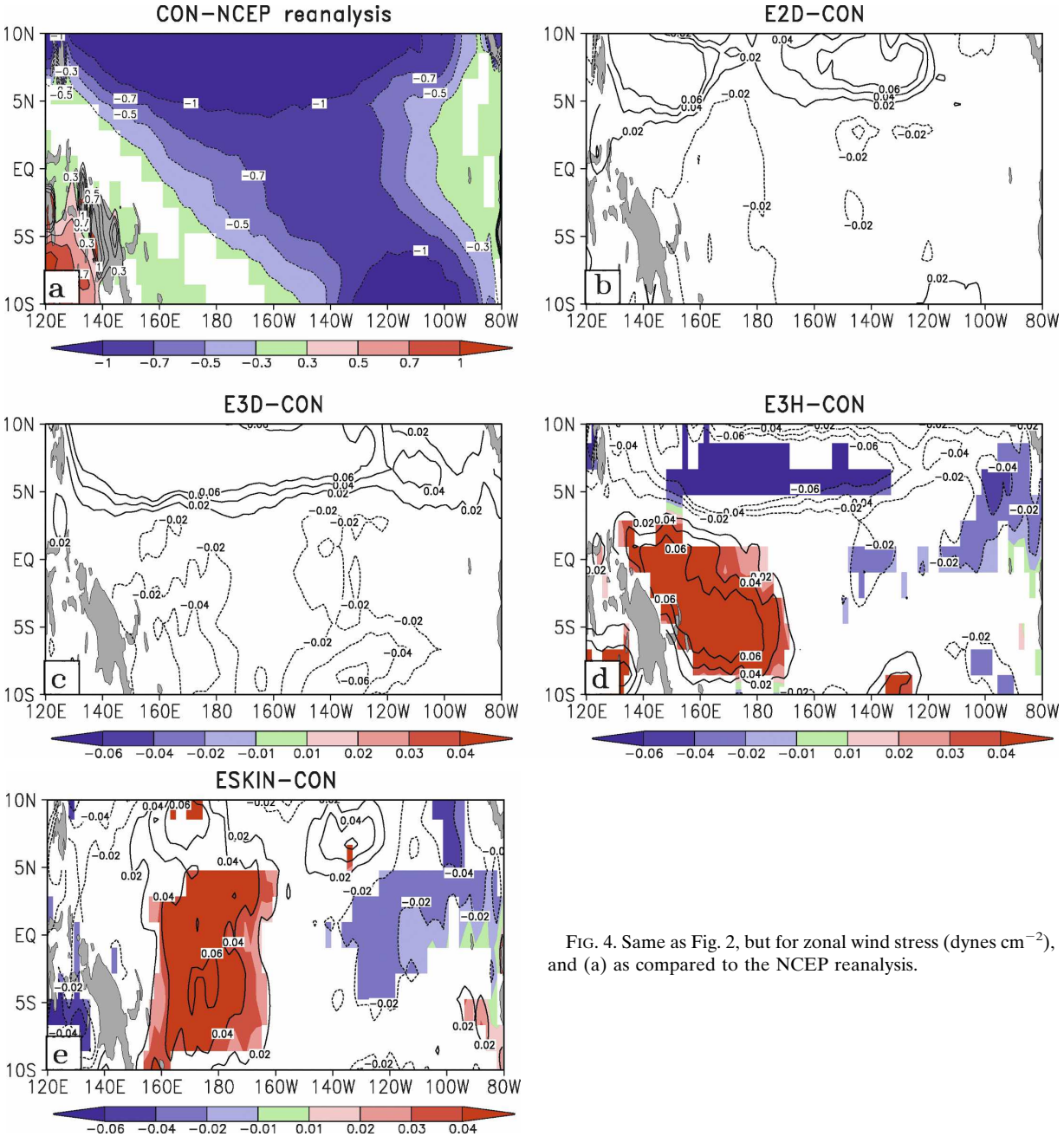

FIG. 4. Same as Fig. 2, but for zonal wind stress (dynes cm^{-2}), and (a) as compared to the NCEP reanalysis.

(Fig. 2e) the cold bias is also reduced in comparison to CON.

These differences in SST are also consistent with differences in the depth of the thermocline (diagnosed as the depth of the 20°C isotherm) shown in Fig. 3. In Fig. 3a we show the bias of the thermocline depth in CON. In comparison to GODAS, the CON has a shallower thermocline over the eastern equatorial Pacific Ocean and in the South Pacific convergence zone. As seen earlier, Figs. 2b,c and Figs. 3b,c also show insignificant differences in the mean state of the thermocline depth in E2D and E3D, respectively, from CON. However, E3H (ESKIN) in Fig. 3d (Fig. 3e) shows a relatively large (marginal) deepening of the eastern equatorial Pacific thermocline depth in comparison to CON.

b. *Zonal wind stress bias*

The climatological mean DJF zonal wind stress errors of the CON are shown in Fig. 4a. The easterly wind

stress bias in the equatorial central and eastern Pacific is consistent with the cold SST bias seen earlier in Fig. 2a. This easterly bias becomes relatively more severe in E2D and E3D, which is also consistent with the colder SSTs seen in Figs. 2b,c relative to the CON. However, as in Figs. 2b,c, these differences remain statistically insignificant. In E3H and ESKIN (Figs. 4d,e), there is a relatively larger reduction in the easterly wind stress bias that is consistent with the corresponding warming of the equatorial Pacific SST seen in Figs. 2d,e, respectively.

c. *East–west equatorial circulation*

The differences in the SST and zonal wind stress can be viewed synergistically with changes in the large-scale east–west (Walker) circulation. In Fig. 5a we show the climatological velocity potential at 200 hPa from the NCEP reanalysis. The ascending cell, where there is upper-level divergence (negative values of 200-hPa velocity potential) over the western Pacific Ocean, and the broad-scale descent, where there is upper-level convergence (positive values of 200-hPa velocity potential) over northern Africa, the Atlantic Ocean, and the tropical eastern Pacific Ocean, are clearly discernible. The corresponding results from the CON are shown in Fig. 5b. The westward extension of the ascending cell of the east–west circulation over the tropical Indian Ocean in the CON run is an unrealistic feature of this model. Misra et al. (2007) showed that this ascent over the Indian Ocean coincides with copious rainfall over the region that is unsupported by observations. Furthermore, the erroneous reduction of convection (and the decrease in ascent) over the western Pacific Ocean also results in a warm SST bias (Fig. 2a). Nonetheless, the region of descent of this east–west circulation and the ascent over the tropical western Pacific Ocean is reasonably well simulated in CON. As seen earlier, E2D and E3D in Figs. 6a,b show an insignificant impact on the large-scale circulation of the CON run. In comparing Figs. 6c and 5b, it is seen that the E3H experiment intensifies the ascending cell (and the descent) of the Walker circulation in the western Pacific (tropical South America) relative to CON. However, the ESKIN experiment accentuates the bias of the CON further (comparing Figs. 6d and 5b), with the ascent over the western Pacific (western equatorial Indian Ocean) reducing (increasing) relative to CON.

As a consequence of this reduction in ascent (convection) over the western Pacific Ocean, ESKIN displays weaker low-level easterlies compared to CON. This is illustrated in Fig. 7, which shows the climatological mean DJF difference between CON and the rest of the four different simulations in 1000-hPa winds overlaid on the corresponding surface pressure difference (after their zonal mean has been removed). As seen before, the differences in the zonal surface pres-

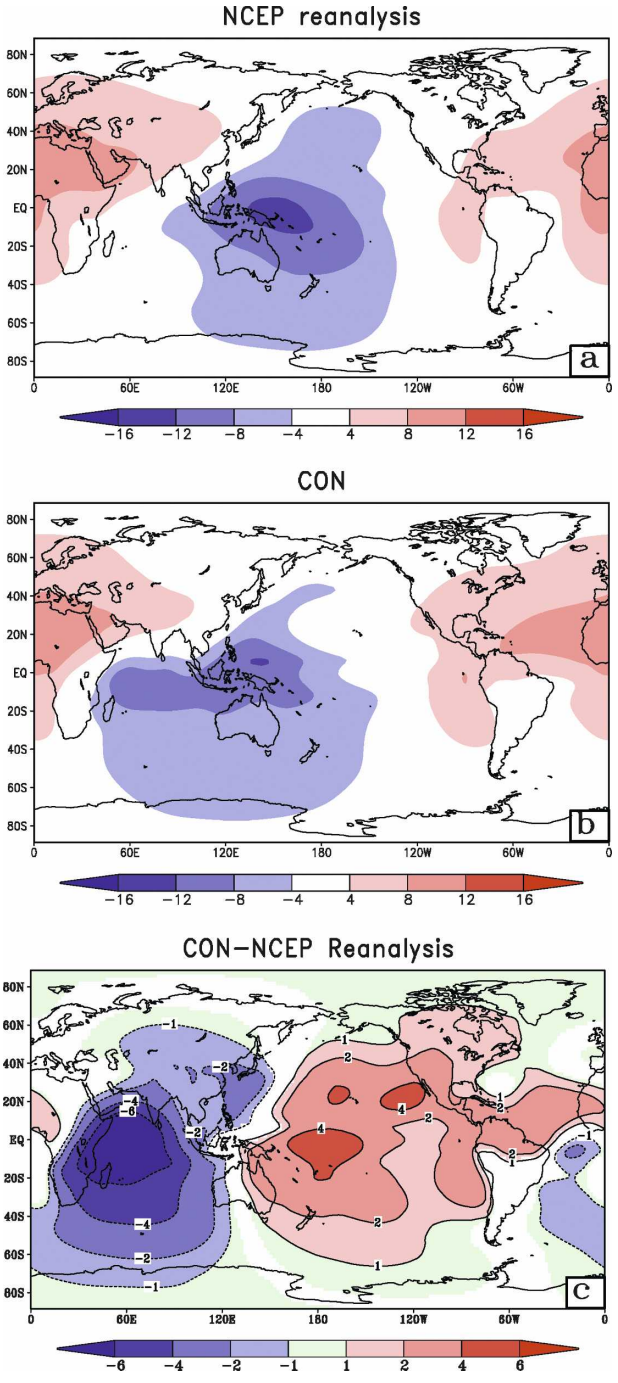

FIG. 5. The climatological mean DJF velocity potential at 200 hPa from (a) the NCEP reanalysis, (b) CON, and (c) their difference with statistically significant values shaded at 90% confidence interval according to the *t* test. Units: 1.0×10^{-6} m^2 s^{-1}.

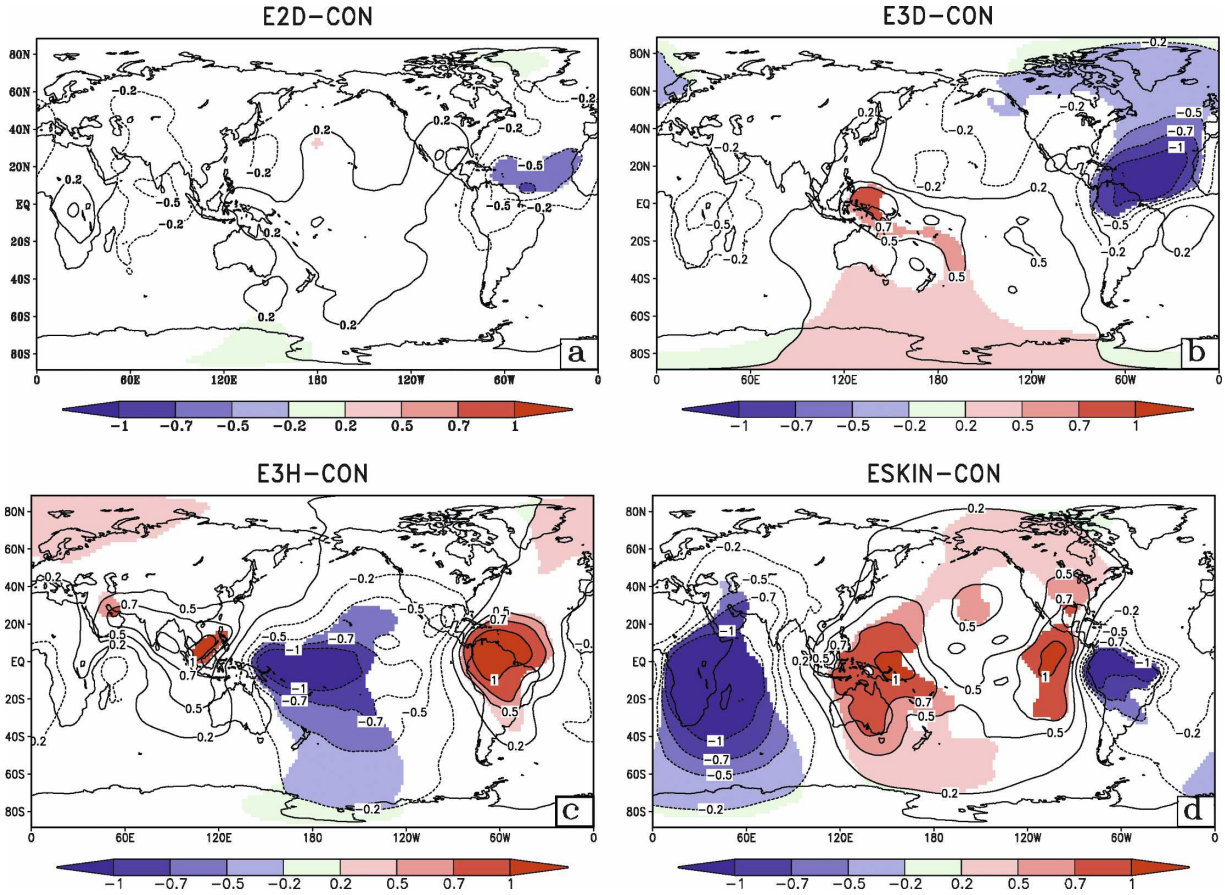

FIG. 6. The climatological mean DJF difference of 200-hPa velocity potential between (a) E2D, (b) E3D, (c) E3H, and (c) ESKIN and CON. Significant values at 90% significance level according to the *t* test are shaded. Units: 1.0×10^{-6} m^2 s^{-1}.

sure gradient and low-level winds over the equatorial Pacific Ocean in E2D (Fig. 7a), E3D (Fig. 7b), and CON are insignificant. This zonal surface pressure gradient has significantly changed in E3H (Fig. 7c) relative to the CON in such a way that the surface easterlies are appreciably reduced over the central equatorial Pacific Ocean. In the ESKIN experiment (Fig. 7d) this east–west surface pressure gradient (between 120°E and 160°W) is reduced as a result of the reduction in ascent over the western Pacific Ocean that results in the weakening of the surface easterlies over the central Pacific Ocean relative to CON.

d. Interannual variability

To understand the implications of the coupling interval on the representation of ENSO variability in the model, Fig. 8 shows the power spectra of the Niño-3.4 SST index following the maximum entropy method of Ghil et al. (2002). It should be noted that all months of the integration were used to calculate this spectra. It is clearly seen from the figure that HadISST1.1 exhibits two distinct peaks in the 2–7-yr range—one around 2.5 yr and the other around the 4-yr period. The CON run produces a peak of around 3 yr, albeit weaker than that of HadISST1.1. The E2D and E3D experiments have a rather flat spectrum in the 2–7-yr range with a small peak in the spectrum around the 2- and 2.5-yr periods, respectively. The E3H and ESKIN show some slight but insignificant strengthening of the CON spectrum with a marginal shift of the peak to higher periods. The spatial structure of this variability in the tropical Pacific is also comparable in these three simulations (not shown).

e. Diurnal forcing

As discussed in the introduction there is a growing body of evidence to suggest that there is rectification by the diurnal variability of the air–sea interactions on longer time scales (Danabasoglu et al. 2006; Bernie et al. 2005, 2007). However, as pointed out in Bernie et al.

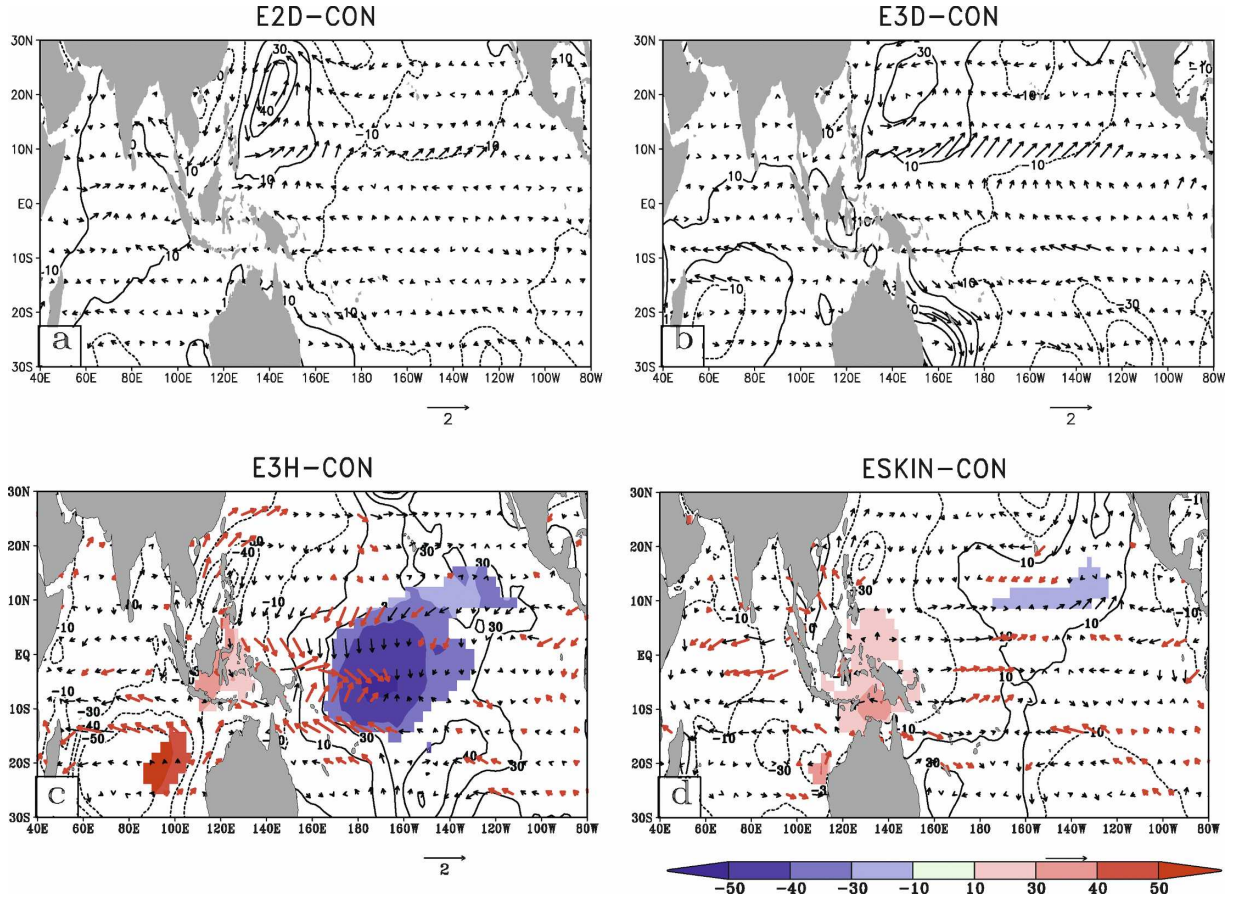

FIG. 7. The climatological mean DJF difference of 1000-hPa winds ($m\ s^{-1}$) and surface pressure (Pa) after its zonal mean has been removed between (a) E2D, (b) E3D, (c) E3H, and (d) ESKIN and CON. The red arrows and shading of surface pressure anomalies indicate significance at 90% significance level according to the *t* test.

(2005, 2007), our OGCM with a 10-m resolution of the topmost ocean layer is incapable of resolving the diurnal variations in the mixed layer of most parts of the tropical oceans despite resolving the diurnal variations of the surface fluxes. This is made apparent by examining the seasonal DJF climatology of the diurnal amplitude ($=T_{max} - T_{min}$) of the bulk (skin) SST in E3H in Fig. 9a (ESKIN in Fig. 9b). These diurnal amplitudes of SST are extremely small compared to that observed (Clayson and Weitlich 2007) or simulated in the high vertical resolution OGCM (Bernie et al. 2007). However, the diurnal amplitude of SST is larger over the eastern equatorial Pacific Ocean in both ESKIN and E3H experiments, consistent with the prevalent light trade winds over the region during the DJF season (Bernie et al. 2007).

The failure of the ESKIN experiment to produce stronger diurnal variations, despite its allowance for very high-frequency air–sea interaction, is also because of its design. The interaction between the skin SST and the bulk SST in ESKIN is "one way": the skin SST is directly influenced by the bulk SST (which is updated once a day) at every time step of the AGCM. However, the skin SST is unable to influence the evolution of the bulk SST at intervals of less than 1 day. Therefore, the OGCM in the ESKIN run does not realize the full effect of the high-frequency air–sea interactions. This is apparent in Fig. 10, which shows the differences between the bulk and the skin SST of the ESKIN experiment over the equatorial Pacific Ocean. Because the evolution of the skin SST in ESKIN is constrained by the influence of the bulk SST, it is seen in Fig. 10 that the differences are marginal, especially over the DJF season. However, it has to be realized that as a result of the cold tongue bias the mean surface easterlies are erroneously strong (not shown), which further diminishes the diurnal variations of the skin SST. In AGCM-only experiments forced with observed SST, this skin SST algorithm shows a much larger diurnal amplitude (Brunke et al. 2008) over the tropical Pacific.

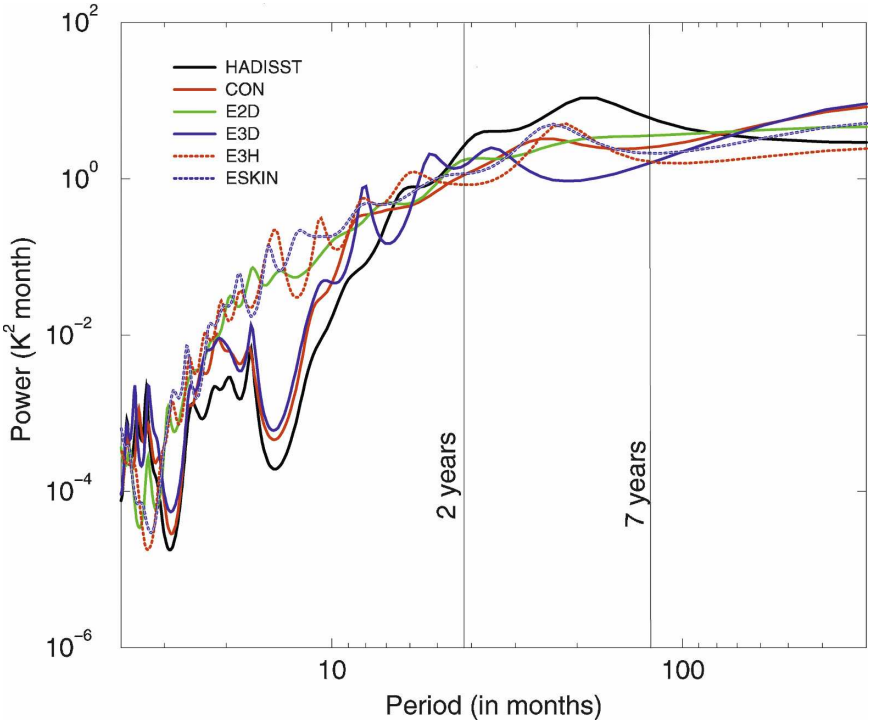

FIG. 8. The maximum entropy spectra of Niño-3.4 SST index. The vertical lines correspond to periods of 2 and 7 yr.

f. Stochastic forcing

In a revealing theoretical model experiment Sura and Penland (2002) showed that the details of the stochastic forcing (its spectrum and distribution) can modulate the low-frequency response of a double-gyre ocean model. In this section it will be argued that the differences in the mean state of the equatorial Pacific between E3H, ESKIN, and CON is largely a result of the change in the atmospheric stochastic forcing facilitated by the change in the frequency of the air–sea coupling.

As a measure of the "atmospheric stochasticity," in Fig. 11 we show the DJF seasonal mean variance of the net heat flux computed from their values stored at the coupling intervals of the respective experiments (see appendix A). Obviously the high-frequency variance is underestimated by averaging it first over the season and then over a 30-yr period. However, it provides a concise and uniform way of comparing the high-frequency variance of the air–sea interaction across these coupled model experiments. We have deliberately chosen the net heat flux over wind stress because its differences are larger between the model simulations. The fluxes were stored at 3-h intervals for a 30-yr window of the 50-yr integration of the E3H. Therefore, to conform to uniformity we have used only 30 yr of flux data from all of the model integrations to compute the variance shown in Fig. 11.

The E2D (Fig. 11b) and E3D (Fig. 11c) experiments have their variances of the net heat flux similar to those of the CON run, except over the eastern equatorial Pacific region (which is probably a reflection of the differences in the mean bias). However, E3H (Fig. l1d) shows a significant increase in the variance over the equatorial Pacific region west of the date line. Likewise, the variance of the net heat flux in the ESKIN in Fig. 11e also increases, albeit marginally over the western equatorial Pacific Ocean relative to CON. We contend that it is the increase in this stochastic forcing of the net heat flux over the western equatorial Pacific Ocean (the ascent region of the Walker circulation) that is critical to the cold tongue bias of the simulation.

As a consequence of this difference in the high-frequency variance of the atmospheric forcing, the transient kinetic energy (TKE) following Sura and Penland (2002; also defined in appendix B) shows interesting differences between the experiments. This is illustrated in Fig. 12, which shows the mean DJF TKE integrated from the surface to the depth of the thermocline. It is clearly seen that the CON run (Fig. 12b) underestimates the TKE in comparison to GODAS (Fig. 12a). E2D in Fig. 12c does not show any significant difference

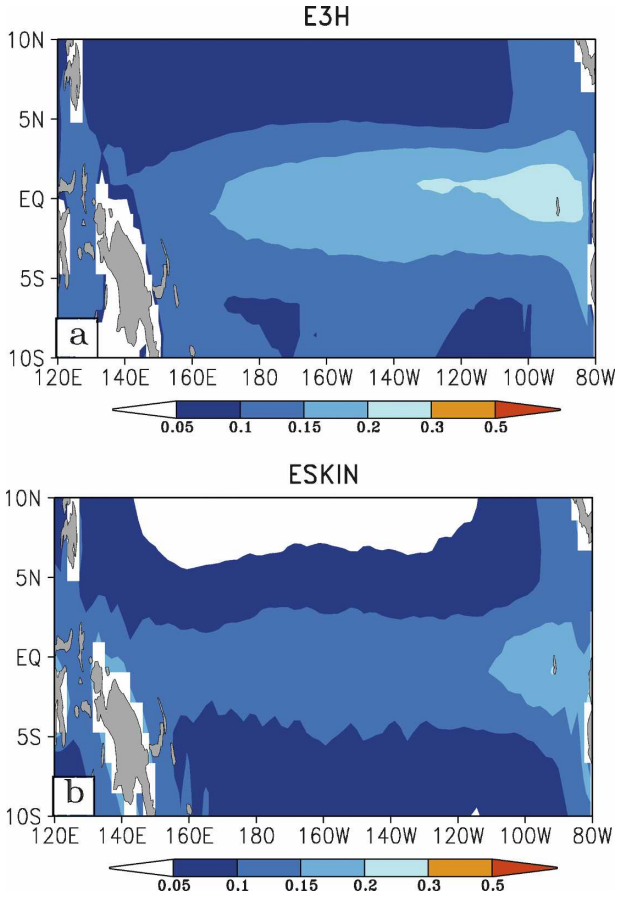

FIG. 9. (a) The DJF seasonal climatology of the diurnal amplitude ($=T_{max} - T_{min}$) of bulk SST (°C) from E3H. (b) Similarly, the diurnal amplitude of the skin SST from ESKIN.

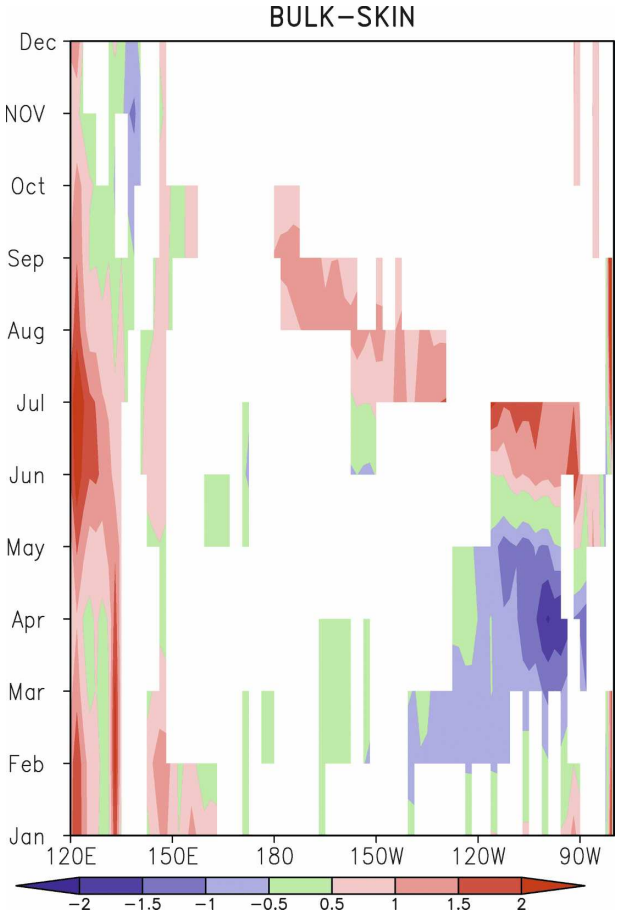

FIG. 10. The climatological monthly mean differences between the bulk and the skin SST over the equatorial Pacific (averaged between 5°S and 5°N) from ESKIN. Shading denotes significant values at 90% confidence interval according to the *t* test.

from the CON run, but the E3D integration (Fig. 12d) shows a decrease in the TKE relative to CON. E3H (Fig. 12e) and ESKIN (Fig. 12f) both display an increase in the TKE over the western equatorial Pacific Ocean in comparison to CON. The corresponding vertical cross section of the TKE along the equatorial Pacific region is shown in Fig. 13. Here, it is consistent with the previous figure (Fig. 12) that the TKE is enhanced (reduced) to the west of the date line through the depth of the thermocline in the E3H and ESKIN (E2D and E3D) experiments relative to CON.

g. Computational time

One of the foremost advantages of the ESKIN experiment over E3H is that it is computationally cheaper. In percentage terms of the wall-clock time of the CON run, E3H takes about 38% more while ESKIN is nearly comparable to the CON integration. E2D and E3D show a marginal reduction in wall-clock time with respect to the CON integration of about 3% and 6%, respectively.

5. Conclusions

This study was motivated to understand if the coupling interval of 1 day between the AGCM and the OGCM in the COLA climate model is an optimal choice. A set of five coupled multidecadal integrations was conducted with different coupling intervals between the AGCM and the OGCM. Two of these experiments attempted to resolve the diurnal scales in the air–sea interaction, namely, E3H and ESKIN. The overwhelming conclusion from this study is that the COLA climate model is rather insensitive to using 1-, 2-, or 3-day coupling intervals. Our initial apprehension of the lack of subseasonal activity in the COLA AGCM was further reinforced by this lack of sensitivity to synoptic coupling intervals. Such an absence of subsea-

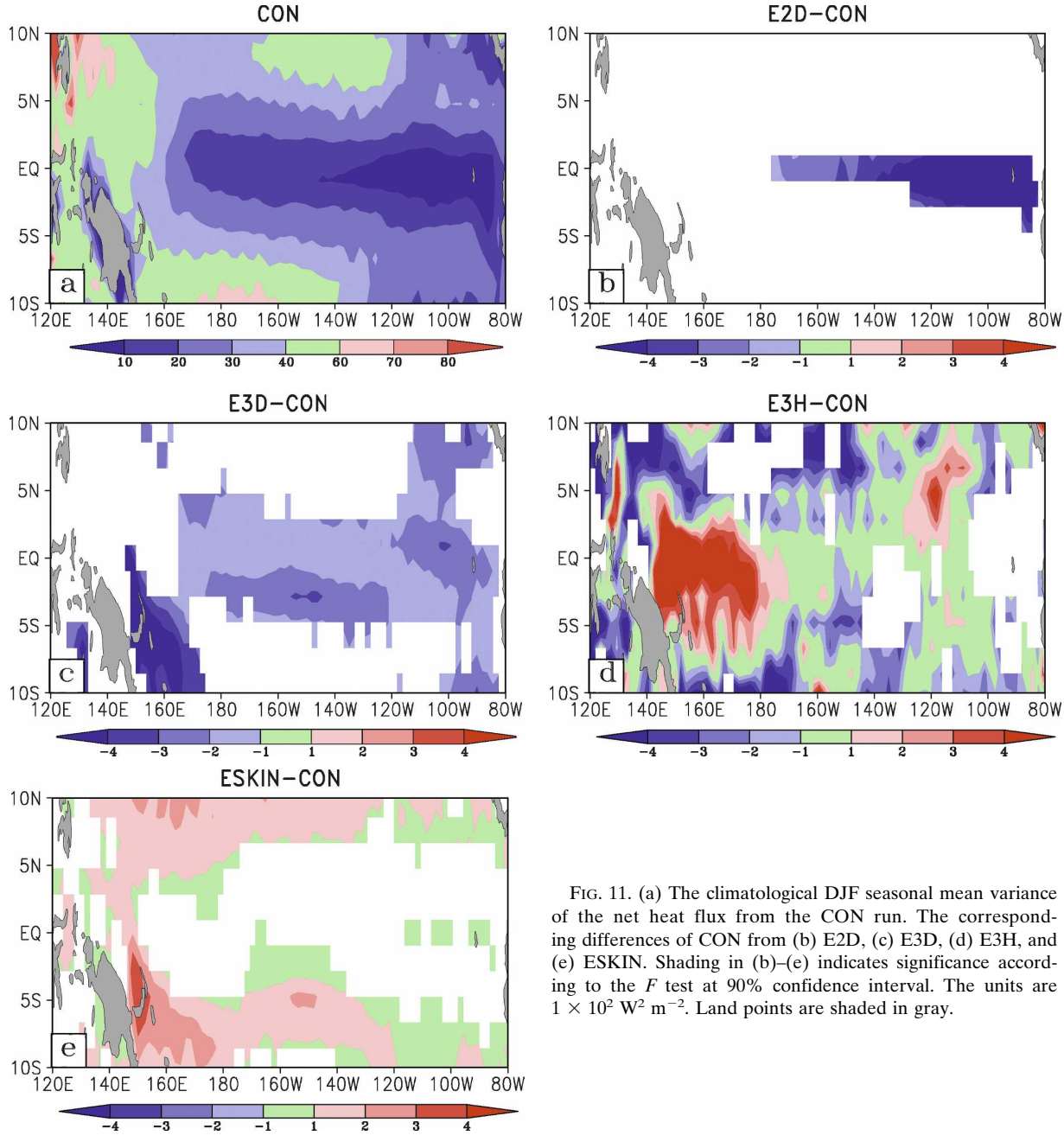

FIG. 11. (a) The climatological DJF seasonal mean variance of the net heat flux from the CON run. The corresponding differences of CON from (b) E2D, (c) E3D, (d) E3H, and (e) ESKIN. Shading in (b)–(e) indicates significance according to the F test at 90% confidence interval. The units are 1×10^2 W^2 m^{-2}. Land points are shaded in gray.

sonal variations in other AGCMs has also been documented (Lin et al. 2006). Therefore, conclusions from this study may have a bearing with respect to other climate models. However, it may be mentioned that there is an indication for a gradual (albeit statistically insignificant) deterioration of the model bias over the equatorial Pacific as the coupling interval is increased from 1 to 2–3 days. This observation is important because when we raised the coupling interval to 5 days (not shown) the cold tongue bias became in excess of 5°C over a 15-yr integration period.

On the other hand, reducing the coupling interval between the AGCM and the OGCM to 3 h resulted in some significant reduction in the model bias. The cold bias of the equatorial Pacific was reduced with a concomitant reduction in the easterly bias of the surface wind stress and eastward shift of the Walker circulation relative to the control (CON). The interannual variabil-

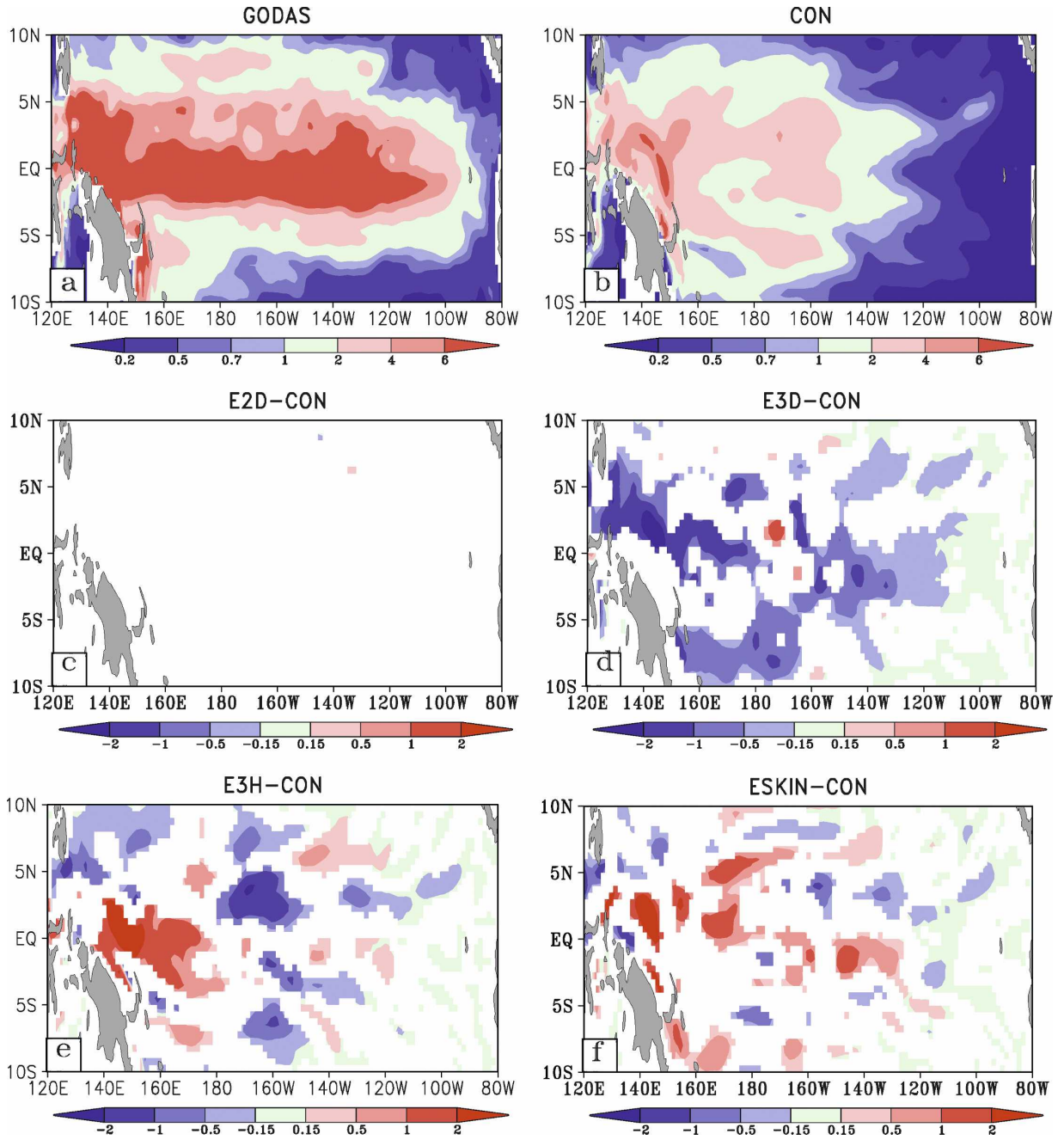

FIG. 12. The TKE (see appendix B) of the upper ocean (up to 400 m below the surface) from (a) GODAS and (b) CON. The difference of the TKE is shown between (b) E2D, (c) E3D, (d) E3H, and (e) ESKIN and CON. Shading in (b)–(e) signifies significance according to the t test at 90% confidence interval. The units are 1×10^{-3} J m^{-2}. Land points are shaded in gray.

ity in the Niño-3.4 region showed much less sensitivity with E3H and ESKIN showing some marginal improvements in the strength and period of ENSO.

The ESKIN experiment, which has the advantage over E3H of being less computationally expensive, displayed some reduction in the cold bias over the equatorial Pacific relative to the CON model. However, unlike E3H, the interaction with the skin SST resulted only in small improvements of the mean bias relative to CON.

The potential benefit of resolving the diurnal variability in the surface fluxes of E3H and ESKIN could not be completely realized because of the coarse vertical resolution of the mixed layer in the OGCM. How-

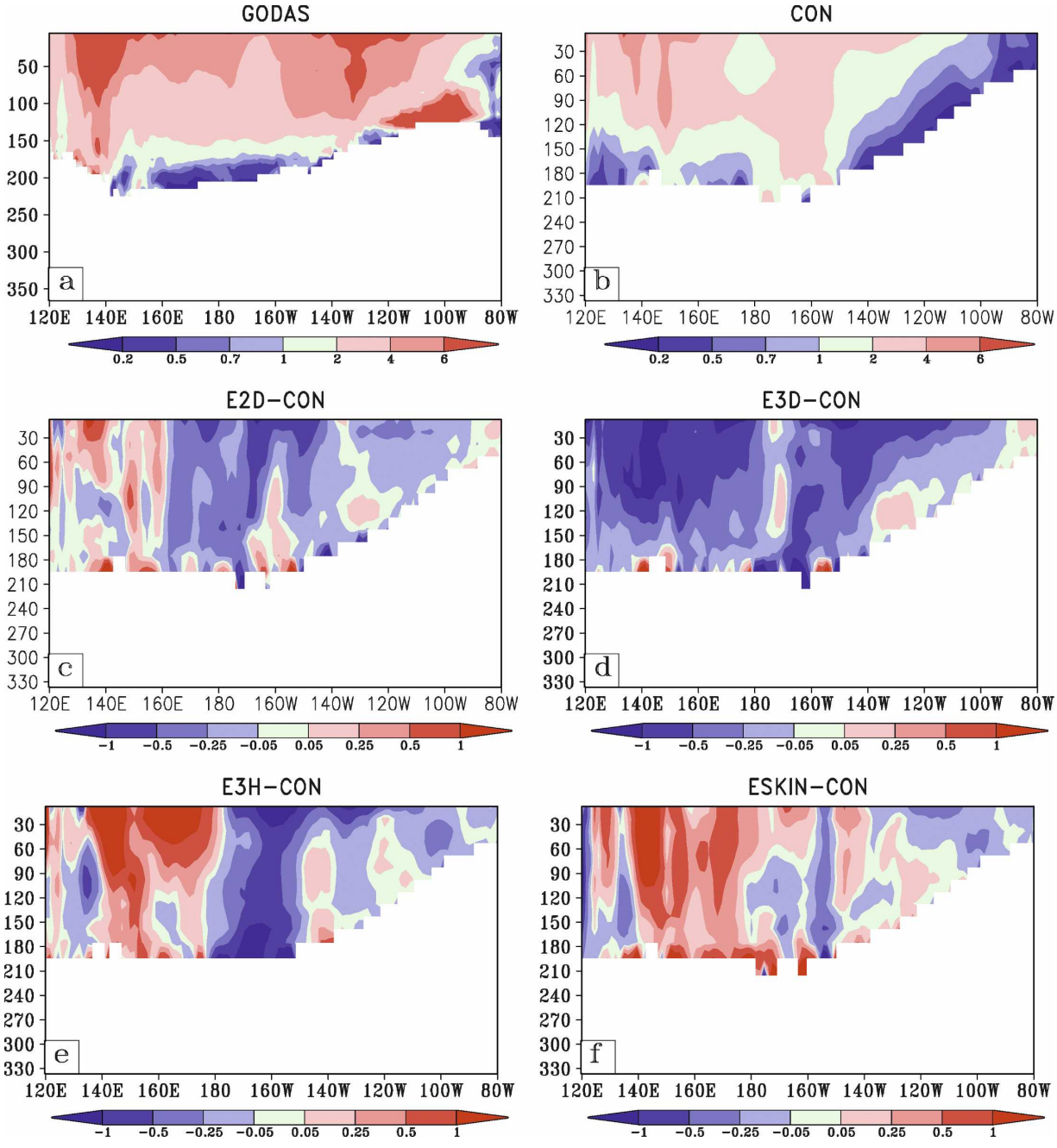

FIG. 13. The equatorial cross section of the TKE of the upper ocean from (a) GODAS and (b) CON. The difference of the TKE is shown between (b) E2D, (c) E3D, (d) E3H, and (e) ESKIN and CON. Shading in (b)–(e) signifies significance according to the t test at 90% confidence interval. The units are 1×10^{-2} J m^{-2}. Land points are shaded in gray.

ever, raising the coupling interval has the additional potential benefit of increasing the stochastic forcing of the atmosphere on the coupled system. This benefit can be realized even in a coarse OGCM, such as that used in this study. In our coupled modeling experiments of E3H and ESKIN, the virtue of this stochastic forcing is seen to ameliorate the mean bias in the E3H and ESKIN. Sura and Penland (2002), in a more simple modeling system, demonstrated that the atmospheric stochastic forcing has the potential to modulate the low-frequency response of the ocean model.

However, it is sobering to note that the rectification implied in the E3H experiment is a fraction of the climatological errors of the CON COLA model over the

equatorial Pacific region. This was also true when the diurnal cycle was resolved in several ways in the CCSM3, which included changing the coupling to both 3 and 1 h (Danabasoglu et al. 2006). This probably suggests that addressing the coupling interval issue alone may not be sufficient to resolve the equatorial cold tongue bias over the Pacific Ocean displayed by the coupled models. The lack of sufficient stratus clouds in the eastern oceans and the bias in the upwelling along the eastern boundaries are some of the other compelling problems in these coupled models that may have further bearing on this cold tongue issue.

Acknowledgments. The authors thank Drs. Christiana Stan and V. Krishnamurthy for making valuable suggestions to improve an earlier version of the manuscript. The lead author is indebted to Dr. Cecile Penland for sharing her wisdom of stochastic forcing on ocean models. The authors are also thankful to two anonymous reviewers for their insightful comments. This study was supported by NSF Grants ATM0332910 and ATM0634762 (to The University of Arizona), NASA Grant NNG04GG46G, and NOAA Grant NA04OAR4310034. The use of computing resources at the NASA Ames facility under NASA Project NNG06GB54G and Columbia Project SMD05-0115 is also acknowledged.

APPENDIX A

Calculation of the Seasonal Variance of the Net Heat Flux

The climatological variance of the net heat flux at the jth sampling (coupling) interval of the model integration is given by

$$V_j = \frac{1}{(N-1)} \sum_{i=1}^{N} (\upsilon_{ij} - \overline{\upsilon_j}), \tag{A1}$$

where N = number of years (= 30), υ_{ij} = net heat flux of the ith year at the jth sampling interval, and $\overline{\upsilon_j} = (1/(N))\Sigma_{i=1}^{N}\upsilon_{ij}$. The sampling interval j is a function of the coupling interval of the air–sea interaction in the integration, which is illustrated in Table A1.

Then the seasonal mean variance S of the net heat flux shown in Fig. 11 is computed as

$$S = \frac{1}{M} \sum_{i=1}^{M} V_j, \tag{A2}$$

where M = is the number of sampling intervals in the DJF season (given in Table A1).

TABLE A1. Values of the indices for the various coupled model experiments.

Experiment	Range of j	No. of sampling interval in the DJF season (M)
CON	j = 1, 2, 3, . . . , 360	90
E2D	j = 2, 4, 6, . . . , 360	45
E3D	j = 3, 6, 9, . . . , 360	30
E3H	j = 1, 2, 3, . . . , 2880	720
ESKIN	j = 1, 2, 3, . . . , 360	90

APPENDIX B

The Computation of the TKE

Here,

$$\text{TKE} = \frac{1}{N} \sum_{j=1}^{N} (\overline{E_j} - \overline{E_c}), \tag{B1}$$

where $\overline{E_j}$ is the seasonally averaged TKE for the jth year and $\overline{E_c}$ is the corresponding climatological seasonal TKE. The monthly mean kinetic energy (E) is calculated as

$$E = \int_{z=1}^{\tau d} [(u - u_c)^2 + (\upsilon - \upsilon_c)^2]\rho \, dz \, , \tag{B2}$$

where $z = 1$ is the ocean surface and τ_d is the depth of the thermocline diagnosed as the depth of the 20° isotherm, u and υ are the monthly mean zonal and meridional components of the ocean currents, u_c and υ_c are the corresponding climatological zonal and meridional components of the ocean currents, ρ is the density of seawater (=1025 kg m^{-3}), and dz is the thickness of the ocean layer.

REFERENCES

Bacmeister, J., P. J. Pegion, S. D. Schubert, and M. J. Suarez, 2000: An atlas of seasonal means simulated by the NSIPP-1 atmospheric GCM. Goddard Space Flight Center, NASA Tech. Memo. 104606, Vol. 17, 194 pp.

Berger, A., 1978: Long-term variations of daily insolation and quaternary climate changes. *J. Atmos. Sci.,* **35,** 2362–2367.

Bernie, D. J., S. J. Woolnough, J. M. Slingo, and E. Guilyardi, 2005: Modeling diurnal and intraseasonal variability of the ocean mixed layer. *J. Climate,* **18,** 1190–1202.

——, E. Guilyardi, G. Madec, J. M. Slingo, and S. J. Woolnough, 2007: Impact of resolving the diurnal cycle in an ocean-atmosphere GCM. Part 1: A diurnally forced OGCM. *Climate Dyn.,* **29,** 575–590, doi:10.1007/s00382-007-0249-6.

Brunke, M. A., C. W. Fairall, X. Zeng, L. Eymard, and J. A. Curry, 2003: Which bulk aerodynamic algorithms are least problematic in computing ocean surface turbulent fluxes? *J. Climate,* **16,** 619–635.

——, X. Zeng, V. Misra, and A. Beljaars, 2008: Integration of a prognostic sea surface skin temperature scheme into weather and climate models. *J. Geophys Res.,* in press.

Cash, B., X. Rodo, and J. L. Kinter III, 2007: Links between tropical Pacific SST and the regional climate of Bangladesh: Role

of the eastern and central tropical Pacific. COLA Tech. Rep. 236, 33 pp. [Available online at ftp://grads.iges.org/pub/ctr/ctr_236.pdf.]

Chao, W. C., and B. Chen, 2004: Single and double ITCZ in an aqua-planet model with constant sea surface temperature and solar angle. *Climate Dyn.,* **22,** 447–459, doi:10.1007/s00382-003-0387-4.

Clayson, C. A., and D. Weitlich, 2007: Variability of tropical diurnal sea surface temperature. *J. Climate,* **20,** 334–352.

Collins, W. D., and Coauthors, 2006: The Community Climate System Model version 3 (CCSM3). *J. Climate,* **19,** 2122–2143.

Danabasoglu, G., W. G. Large, J. J. Tribbia, P. R. Gent, and B. P. Briegleb, 2006: Diurnal coupling in the tropical oceans of CCSM3. *J. Climate,* **19,** 2347–2365.

Delsole, T., M. Zhao, P. A. Dirmeyer, and B. P. Kirtman, 2008: Empirical correction of a coupled land–atmosphere model. *Mon. Wea. Rev.,* **136,** 4063–4076.

Dirmeyer, P. A., and F. J. Zeng, 1999: Precipitation infiltration in the simplified SiB land surface scheme. *J. Meteor. Soc. Japan,* **77,** 291–303.

Fairall, C. W., E. F. Bradley, J. S. Godfrey, G. A. Wick, and J. B. Edson, 1996a: Cool-skin and warm-layer effects on sea surface temperature. *J. Geophys. Res.,* **101,** 1295–1308.

——, ——, D. P. Rogers, J. B. Edson, and G. S. Young, 1996b: Bulk parameterization of air-sea fluxes for Tropical Ocean-Global Atmosphere Coupled-Ocean Atmosphere Response Experiment. *J. Geophys. Res.,* **101,** 3747–3764.

Gent, P. R., and J. C. McWilliams, 1990: Isopycnal mixing in ocean circulation models. *J. Phys. Oceanogr.,* **25,** 150–155.

Ghil, M., and Coauthors, 2002: Advanced spectral methods for climatic time series. *Rev. Geophys.,* **40,** 1003, doi:10.1029/2000RG000092.

Hong, S. Y., and H. L. Pan, 1996: Nonlocal boundary layer vertical diffusion in a medium range forecast model. *Mon. Wea. Rev.,* **124,** 2322–2339.

Kalnay, E., and Coauthors, 1996: The NCEP/NCAR 40-Year Reanalysis Project. *Bull. Amer. Meteor. Soc.,* **77,** 437–471.

Kiehl, J. T., J. J. Hack, G. Bonan, B. A. Boville, D. L. Williamson, and P. J. Rasch, 1998: The National Center for Atmospheric Research Community Climate Model: CCM3. *J. Climate,* **11,** 1131–1149.

Kirtman, B. P., and E. Schneider, 2000: A spontaneously generated tropical atmospheric general circulation. *J. Atmos. Sci.,* **57,** 2080–2093.

——, and J. Shukla, 2002: Interactive coupled ensemble: A new coupling strategy for GCMs. *Geophys. Res. Lett.,* **29,** 1367, doi:10.1029/2002GL014834.

——, K. Pegion, and S. M. Kinter, 2005: Internal atmospheric dynamics and tropical Indo-Pacific climate variability. *J. Atmos. Sci.,* **62,** 2220–2233.

Large, W. G., J. C. McWilliams, and S. C. Doney, 1994: Oceanic vertical mixing: A review and a model with a nonlocal boundary layer parameterization. *Rev. Geophys.,* **32,** 363–403.

Latif, M., and Coauthors, 2001: ENSIP: The El Niño simulation intercomparison project. *Climate Dyn.,* **18,** 255–272.

Lin, J. L., and Coauthors, 2006: Tropical intraseasonal variability in 14 IPCC AR4 climate models. Part I: Convective signals. *J. Climate,* **19,** 2665–2690.

Luo, J.-J., S. Masson, E. Roeckner, G. M. Adec, and T. Yamagata, 2005: Reducing climatology bias in an ocean–atmosphere CGCM with improved coupling physics. *J. Climate,* **18,** 2344–2360.

Mechoso, C. R., and Coauthors, 1995: The seasonal cycle over the tropical Pacific in coupled ocean–atmosphere general circulation models. *Mon. Wea. Rev.,* **123,** 2825–2838.

Misra, V., and L. Marx, 2007: Manifestation of remote response over the equatorial Pacific in a climate model. *J. Geophys. Res.,* **112,** D20105, doi:10.1029/2007JD008597.

——, and Coauthors, 2007: Validating and understanding ENSO simulation in two coupled climate models. *Tellus,* **59A,** 292–308.

——, L. Marx, M. Fennessey, B. Kirtman, and J. L. Kinter III, 2008: A comparison of climate prediction and simulation over tropical Pacific. *J. Climate,* **21,** 3601–3611.

Moorthi, S., and M. J. Suarez, 1992: Relaxed Arakawa–Schubert: A parameterization of moist convection for general circulation models. *Mon. Wea. Rev.,* **120,** 978–1002.

Pacanowski, R. C., and S. M. Griffies, 1998: MOM3.0 manual. NOAA/Geophysical Fluid Dynamics Laboratory, 638 pp.

Randall, D. A., and Coauthors, 2007: Climate models and their evaluation. *Climate Change 2007: The Physical Science Basis,* S. Solomon et al., Eds., Cambridge University Press, 591–648.

Rao, A. K., and K. R. Sperber, 2006: ENSO simulation in coupled ocean-atmosphere models: Are the current models better? *Climate Dyn.,* **27,** 1–15.

Rayner, N. A., D. E. Parker, E. B. Horton, C. K. Folland, L. V. Alexander, D. P. Rowell, E. C. Kent, and A. Kaplan, 2003: Global analyses of sea surface temperature, sea ice, and night marine air temperature since the late nineteenth century. *J. Geophys. Res.,* **108,** 4407, doi:10.1029/2002JD002670.

Redi, M. H., 1982: Oceanic isopycnal mixing by coordinate rotate. *J. Phys. Oceanogr.,* **12,** 1154–1158.

Saha, S., and Coauthors, 2006: The NCEP Climate Forecast System. *J. Climate,* **19,** 3483–3517.

Smagorinsky, J., 1963: General circulation experiments with the primitive equations: I. The basic experiment. *Mon. Wea. Rev.,* **91,** 99–164.

Sperber, K. R., S. Gualdi, S. Legutke, and V. Gayler, 2005: The Madden–Julian oscillation in ECHAM4 coupled and uncoupled general circulation models. *Climate Dyn.,* **25,** 117–140, doi:10.1007/s00382-005-0026-3.

Sumi, A., 1992: Pattern formation of convective activity over the aqua-planet with globally uniform sea surface temperature. *J. Meteor. Soc. Japan,* **70,** 855–876.

Sura, P., and C. Penland, 2002: Sensitivity of a double-gyre ocean model to details of stochastic forcing. *Ocean Modell.,* **4,** 327–345.

Tiedtke, M., 1984: The effect of penetrative cumulus convection on the large-scale flow in a general circulation model. *Beitr. Phys. Atmos.,* **57,** 216–239.

Webster, P. J., C. A. Clayson, and J. A. Curry, 1996: Clouds, radiation, and the diurnal cycle of sea surface temperature in the tropical western Pacific. *J. Climate,* **9,** 1712–1730.

Wu, Z., E. K. Schneider, and B. P. Kirtman, 2004: Causes of low frequency North Atlantic SST variability in a coupled GCM. *Geophys. Res. Lett.*, **31,** L09210, doi:10.1029/2004GL019548.

Xue, Y.-K., P. J. Sellers, J. L. Kinter III, and J. Shukla, 1991: A simplified Biosphere Model for global climate studies. *J. Climate,* **4,** 345–364.

——, F. J. Zeng, and C. A. Schlosser, 1996: SSiB and its sensitivity to soil properties: A case study using HAPEX-Mobilhy data. *Global Planet. Change,* **13,** 183–194.

Yu, J.-Y., and C. R. Mechoso, 1999: Links between annual variations of Peruvian stratocumulus clouds and of SST in the eastern equatorial Pacific. *J. Climate,* **12,** 3305–3318.

Zeng, X., and A. Beljaars, 2005: A prognostic scheme of sea surface skin temperature for modeling and data assimilation. *Geophys. Res. Lett.,* **32,** L14605, doi:10.1029/2005GL023030.

——, M. Zhao, R. E. Dickinson, and Y. He, 1999: A multiyear hourly sea surface skin temperature data set derived from the TOGA TAO bulk temperature and wind speed over the tropical Pacific. *J. Geophys. Res.,* **104,** 1525–1536.

Zhang, C., 2005: Madden-Julian Oscillation. *Rev. Geophys.,* **43,** RG2003, doi:10.1029/2004RG000158.

Zhang, G. J., and N. A. McFarlane, 1995: Sensitivity of climate simulations to the parameterization of cumulus convection in the Canadian Climate Centre general circulation model. *Atmos.–Ocean,* **33,** 407–446.

——, and M. Mu, 2005: Effects of modification to the Zhang-McFarlane convection parameterization on the simulation of the tropical precipitation in the National Center for Atmospheric Research Community Climate Model, version 3. *J. Geophys. Res.,* **110,** D09109, doi:10.1029/2004JD005617.

——, and H. Wang, 2006: Toward mitigating the double ITCZ problem in NCAR CCSM3. *Geophys. Res. Lett.,* **33,** L06709, doi:10.1029/2005GL025229.